Journal of Flow Chemistry (2019) 9:175–185
https://doi.org/10.1007/s41981-019-00039-8

FULL PAPER

Experiments on the magnetic enrichment of rare-earth metal ions in aqueous solutions in a microflow device

K. Kolczyk-Siedlecka[1] · M. Wojnicki[1] · X. Yang[2] · G. Mutschke[2] · P. Zabinski[1]

Received: 16 April 2019 / Accepted: 15 May 2019 / Published online: 29 May 2019

Abstract

An attempt is made to achieve a continuous enrichment of rare-earth metal ions from aqueous solutions in a microflow device by applying magnetic forcing. An aqueous solution containing holmium(III) ions is pumped through a small channel which was exposed to a strong inhomogeneous magnetic field. At the outflow, the near- and far-field parts of the flow are separated and analyzed using UV-Vis spectroscopy. The relative change of ion concentration is determined from the measured absorbance. Results are reported for three different types of flow cells at different flow rates and magnetic field strengths and for a cascaded application of cells. The change of concentration is found to be small, and no clear trend can currently be stated due to the error margin of the concentration measurement.

Keywords Microflow · Spectrophotometry · Rare-earth elements · Magnetic field · Continuous separation

Introduction

High Gradient Magnetic Separation (HGMS) is arousing increasing interest as a technology that can replace or support currently applied methods of metal production thanks to its low costs, low energy consumption, easy application, increased efficiency and other aspects. The issue has been investigated by scientists for several years. The processes under discussion are used in the separation of metals in ionic form, in a liquid phase and in a mixture of phases, e.g. in the form of nanoparticles. Using the magnetic field enables the elimination of ions and solid particles with paramagnetic and ferromagnetic properties. Separation under the magnetic field can be used in medicine, diagnostics [1], molecular biology and other biological sciences [2–5]. This method can also be applied in waste water purification [6–8] and hydrometallurgical [9] or recycling [10] processes, both at the initial and final stages, e.g. in the concentration of ores and solutions, or in the separation of ion mixtures into individual ions. Recently, the separation of ions with different magnetic properties has become a progressively popular issue. Among other things, the direct separation of ions allows solutions of certain metals to be concentrated with no need for nanoparticle synthesis or processes of adsorption and desorption on their surface which can make the processes last longer. Scientific works have dealt with the separation of ions of metals displaying ferromagnetic properties (Fe) [11] or ions of rare-earth metals (REMs) [10, 12–17].

The group of rare-earth elements (REEs) has aroused special interest in research works due to their wide application in modern technologies [18–20] and hindered production processes. The most difficult production stage is separation, because of their high chemical similarity.

Highlights
- The influence of a magnetic field gradient on the transport of Ho(III) ions in microflow cells was studied.
- The magnetic field gradient dependent on the orientation of the cell in the magnetic field was simulated. The distribution of Ho(III) ions is analyzed using UV/Vis spectroscopy.
- A detailed analysis of different aspects influencing ion transport in the continuous flow process is presented.

Electronic supplementary material The online version of this article (https://doi.org/10.1007/s41981-019-00039-8) contains supplementary material, which is available to authorized users.

✉ K. Kolczyk-Siedlecka
kkolczyk@agh.edu.pl

[1] Faculty of Non-Ferrous Metals, AGH University of Science and Technology, al. Mickiewicza 30, 30-059 Krakow, Poland

[2] Institute of Fluid Dynamics, Helmholtz-Zentrum Dresden-Rossendorf (HZDR), Bautzner Landstr. 400, 01328 Dresden, Germany

Rare-earth metals are both recycled and produced through the hydrometallurgical method. Therefore, it is necessary to apply complicated processes using different extractants, often accompanied by toxicity and high costs [21, 22].

There are ions with para- and diamagnetic properties among the REMs, so it is possible to divide them into two groups of different properties from a mixture of ions. To determine the possibility of HGMS working on REE ions, it is necessary to make a preliminary analysis of single metal solutions. Current research is focused on analyzing the transport of REE ions in a static state. Works [12, 13] analyzed the change in the concentration of Dy(III) ions under the magnetic field generated by a neodymium magnet placed on the top of the solution. In other works [14, 15] the separation was analyzed in a Ho(III) solution. In these cases, neodymium magnets were placed at the bottom of the solution. In work [16] the experimental set was very similar to the previous case, but gelatin gel was used to decrease the spontaneous diffusion generated by concentration differences. Work [17] presents results connected with the analysis of the magnetomigration of Dy(III) and Y(III) ions. Work [23] analyzed the mechanism of Dy(III) ion transportation under the gradient of the magnetic field. It ascertained that the enrichment of the concentration in the upper part of the solution is connected with the evaporation of water.

The magnetic separation of ions and solid particles or colloidal suspensions differs due to the type of interactions between individual ions or solid particles with a disperser or solvent. This situation is connected with the challenge of finding optimal parameters for these processes. The motivation of this work is to analyze the separation of rare-earth metals in aqueous solutions in a continuous flow process where the transport of paramagnetic ions is influenced by a strong magnetic gradient force. The natural first step is to study single salt solutions. In this work, a holmium solution was analyzed because of the high magnetic moment of Ho(III) ions.

Experiment and simulations

Chemical reagents

Dry $HoCl_3$ salt (Oxymet.com, 99.9%) was dissolved into deionized water to obtain a 0.1 M concentration of holmium ions. The element holmium was chosen as it has the highest value of magnetic momentum [24] in connection with the strongest paramagnetic properties of all the REE ions at +3 level of oxidation. Hydrochloric acid (Chemsolute, 32%) was added to the solution to obtain a pH equal to 1. The solution has an acidic pH, this lowers the risk of holmium hydroxide precipitation.

Experimental setup

The idea of the cell design is to achieve a strong gradient of the magnetic field in the cross section of the channel and all along it. To achieve this, an iron wire is arranged close by along the channel, and is magnetized in an external magnetic field, thereby creating the desired strong gradient. Because of the limited space available between the pole shoes of the electromagnets, both the channel and the wire are arranged in a spiral. Different cells were designed with the help of the SolidWorks 2016 software and printed using the Formlabs Form 2 3D printer with light hardened resin (Grey – GPGR03 or Clear – GPCL02), which is chemically resistant to the solutions used. A drawing of the flow cell is shown in Fig. 1. Prior to the experiments, the cell was washed with the holmium solution to avoid the influence of possible adsorption of Ho(III) ions at the channel surface from collected samples.

At the center of the spiral, the solution enters the channel. At the end of the channel, a Y-shaped stream splitter (angle 60^{o}) is placed to separate the two fractions of the flow which are near the iron wire (Output 1) and further away from it (Output 2). The channel is 1 m long. The wire placed parallel along the channel has a diameter of 1 mm and consists of steel type 1.4510 according to the European standard (EN 10088–2:2005).

Three different types of spiral cell with different cross sections were used and are shown in Fig. 2. In Model 1, the circular cross section of the channel has a diameter of 1 mm. Model 2 and Model 3 both have a rectangular cross section of 4×1 mm in size, and the iron wire is placed beside or above the channel, respectively. The distance between the iron wire and the channel is 0.5 mm (Model 1) and 0.1 mm (Model 2 and Model 3). The cells were placed vertically in an electromagnet as shown in Fig. 3.

Additionally, there was created a cascaded setup of three cells with a circular cross section (Model 1) to achieve a greater enrichment effect. The cells were positioned and connected according to the scheme shown in Fig. 4. The solution is introduced into the input of cell 1. Then the outputs near and far from the iron wire are connected to cells 2 and 3, respectively. Thus, at the output, four fractions of the flow are obtained. The maximum and minimum concentration of ions are expected at outputs 1 and 3, respectively.

Two electromagnets from Lake Shore Cryotronics, Inc. (Model 642) and from Schueler Magnetic Ltd. (Model 1000A) were used to generate a homogeneous magnetic field in the intensity range from 0.3 to 0.9 T. All cells were placed in the center between the large pole shoes to avoid the influence of fringe fields. In order to avoid temperature variations, the cell was placed in a Styrofoam container separating it from direct contact with the magnet poles.

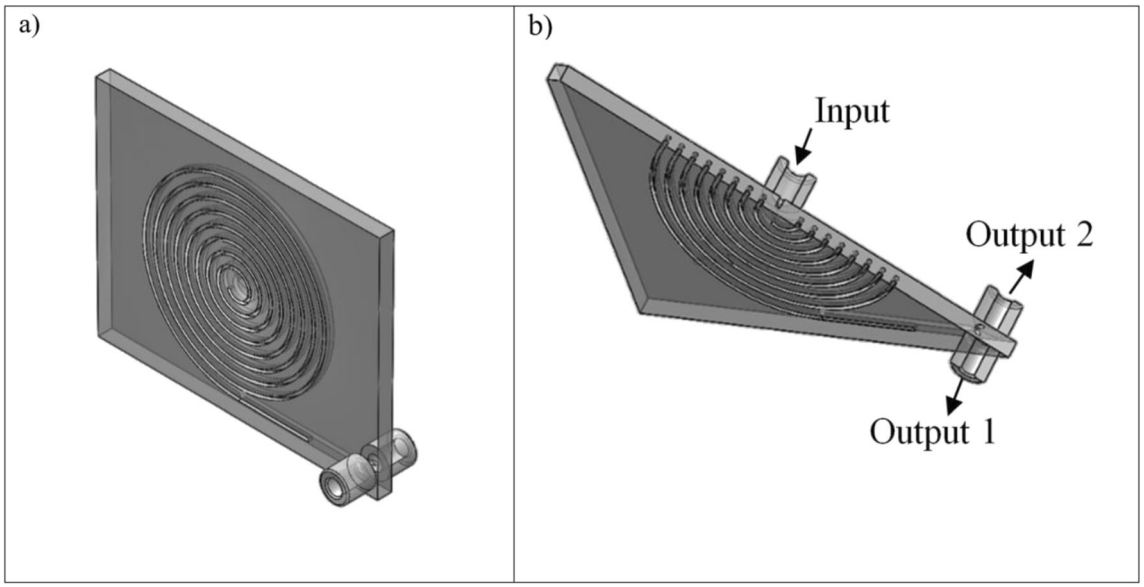

Fig. 1 Drawing of a microflow cell: **a** total picture and **b** cross section

A syringe pump (Ascor AP15) was used to generate different flow rates ranging from 10 to 100 ml/h. To connect the syringe with the cells and the sample jars, PE pipes with an inner diameter of 1 mm and equipped with connectors were used. Samples of about 4 ml solution from the outputs were collected and analyzed employing the UV-Vis spectroscopy method described below.

Simulations of the field gradients

The aim of the present work is to separate the REE ions in a dynamic state. Separation in a magnetic field is based on applying the field force to transport the metals ions. Meanwhile, the magnetic force is generated by the field gradient, which is necessary to enforce the transport of paramagnetic ions. The magnetic force is determined by:

$$\boldsymbol{F}_{mag} = \frac{\Delta\chi V_p}{\mu_0}\,\mathbf{B}\nabla\boldsymbol{B} \tag{1}$$

where $\Delta\chi = \chi_{ion} - \chi_{sol}$ define the difference in the magnetic susceptibility of the ions and solution [−], V_p – volume of particles [m^3], $\mu_0 = 4\pi \times 10^{-7}$ is the magnetic permittivity of vacuum [Hm^{-1}], $\boldsymbol{B}\nabla\boldsymbol{B}$ – magnetic field gradient [$T^2\ m^{-1}$].

In order to optimize the experimental setup, a simulation was performed of the magnetic field distribution and the created gradient of the magnetic field depending on the location of

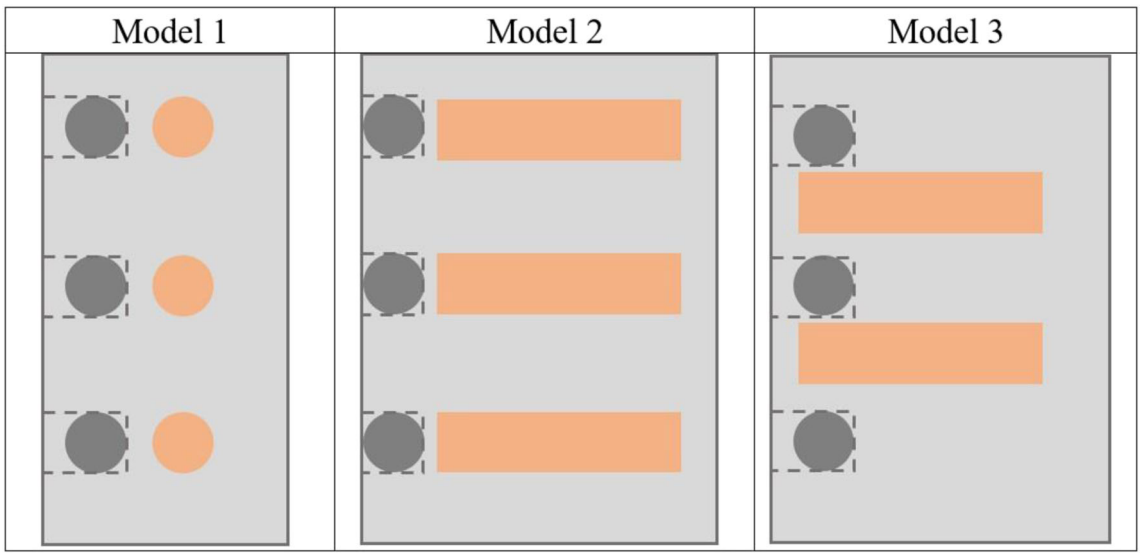

Fig. 2 Cross section of the flow cells (grey – iron wire, orange – channel)

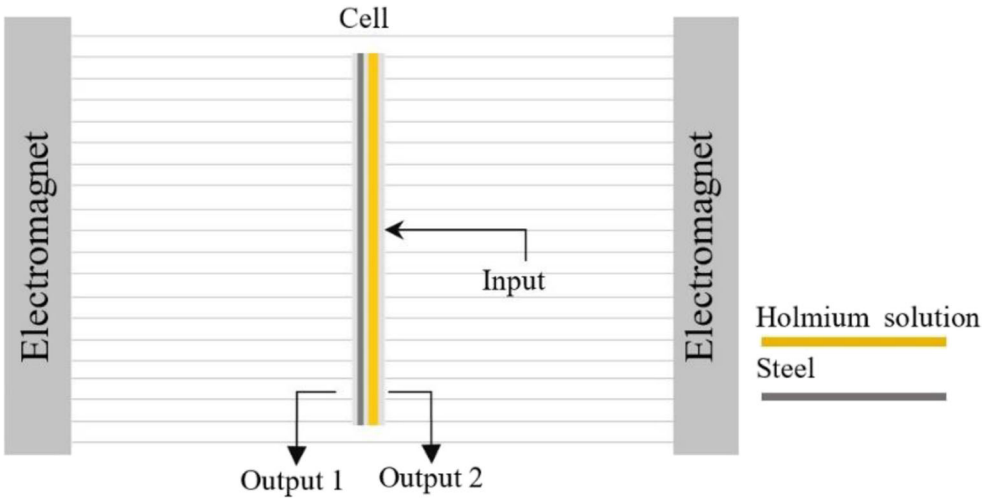

Fig. 3 Sketch of the cell placed in the electromagnet

the channel and steel cord in relation to the direction of the homogeneous magnetic field. The main area of interest is the cross section of the channel in which the solution is transferred. Here, large differences of the magnetic gradient force across the cross-section are desirable for a maximum separation effect. Two cases were analyzed – the cell was placed horizontally or vertically in the external horizontal magnetic field.

The calculations assumed that the intensity of the homogeneous magnetic field is 0.5 T. As this is far below the saturation magnetization of iron (about 2.2 T), a linear constitutive relation can be applied, i.e. $\mathbf{B} = \mu_0\mu_r\,\mathbf{H}$, and a relative magnetic permittivity of 4000 used for iron. The remaining volume can be treated as air ($\mu_r = 1$). The diameter of the steel cord is 1 mm.

The simulations were performed in a 2D rectangular plane normal to the axial direction of the pipe and the iron wire using the software package Comsol Multiphysics ver. 5.3. The magnetostatic problem can be stated as a Laplace equation for the vector potential of the magnetic field:

$$\Delta \boldsymbol{A} = 0, \qquad \boldsymbol{B} = \nabla \times \boldsymbol{A} \tag{2}$$

The external constant magnetic field in either a horizontal or vertical direction can easily be defined as a background magnetic potential. The problem then has to be solved in conjunction with corresponding boundary conditions, which consist in $\mathbf{n} \times \mathbf{H} = 0$ at the two sides normal to the external field direction and $\mathbf{n} \times \mathbf{A} = 0$ at the two sides parallel to it. Due to the 2D character of the problem, finally only a single component of **A** in a direction normal to the 2D plane remains.

Figure 5a shows the distribution of the magnetic field gradient on the cell with a circular channel cross section. The iron, as a ferromagnetic material, attracts the magnetic field, which is instrumental in obtaining a gradient in the channel sections (the black circles) (Fig. 6).

The magnetic force, according to eq. (1), linearly depends on $|\mathbf{B}\nabla\mathbf{B}|$. Therefore, the configuration presented in Fig. 5b, where the cell is placed vertically, is favored due to both the intensity and the magnetic field gradient, and is used for further experiments.

The magnetic field was simulated for two more cells models with the rectangular channel.

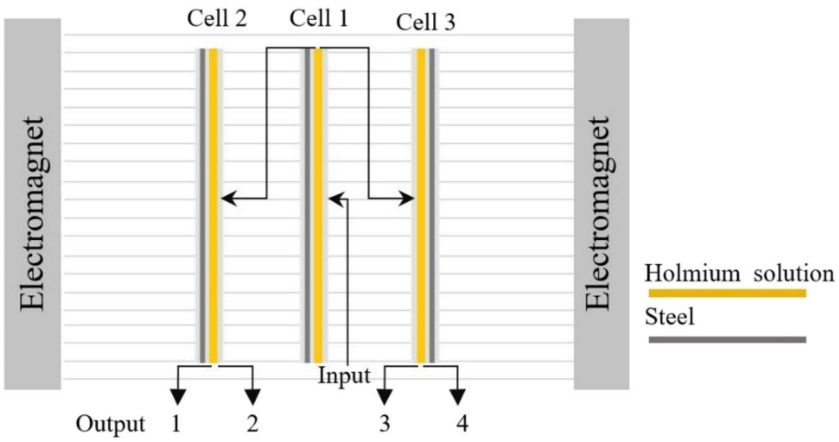

Fig. 4 Sketch of three cascaded cells placed in the electromagnet

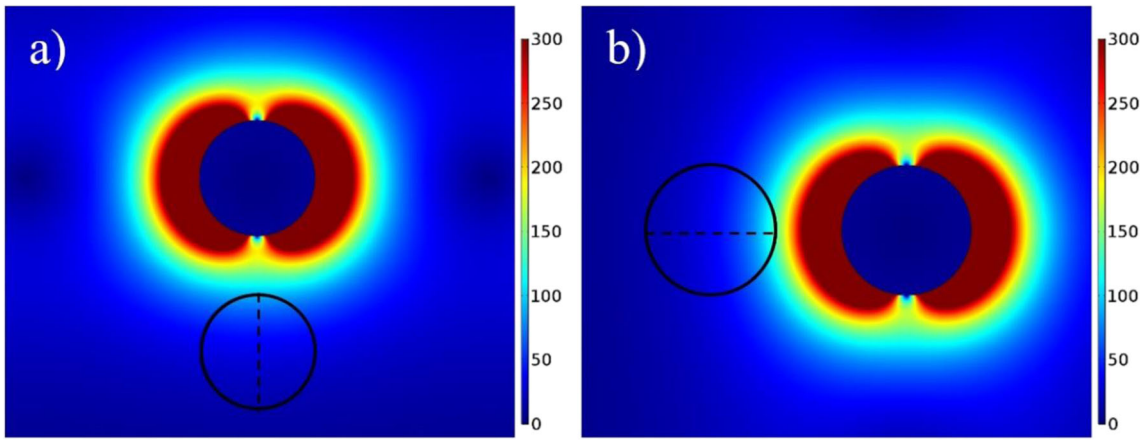

Fig. 5 Simulation of the magnetic field gradient $|\mathbf{B}\nabla\mathbf{B}|$ in T^2/m for two cases: the cell placed (**a**) horizontally and (**b**) vertically. The maximum value shown is limited to improve the presentation

Figure 7 presents the simulation of the magnetic field gradient. The white arrows visualize the direction of the gradient. Empirically, in Model 2 a stronger enrichment in the cell part next to the iron wire can be expected compared to Model 3 (Fig. 8).

Method of analysis

It is well known that Ho(III) ions absorb the light in the UV-Vis spectrum range. Therefore, the obtained solutions were analyzed using UV-Vis spectroscopy (Jasco V-770 and Shimadzu UV-2700 spectrophotometers). For this purpose, 10 mm quartz cuvettes (Hellma Analytics) were used. This method was used as it enables the solutions to be analyzed without diluting the samples. It is one of the most precise methods available (see supplementary materials). After the calibration of the baseline, the standard deviation is equal to 0.0915%. There are distinct local peaks in the absorption spectra, which allows the Ho(III) concentration to be measured accurately.

An example of the UV-Vis spectra curve is shown in Fig. 9. The backgrounds of the UV-Vis spectra measured were corrected using the mean value of absorbance in the wavelength interval of 590–610 nm (area C in Fig. 9). The corrections were made in this wavelength range because in this area there is no absorption of light. This correction allows the background shift to be eliminated. The shift which is observed is probably related to the fact that there are slight differences between the positions of the cuvettes (deviations in their perpendicularity, etc.). The height of the absorbance spectra was compared at two wavelengths: 537 and 641 nm, marked as points A and B in Fig. 9. The measurements were made in a scanning range of 700–300 nm with 0.1 nm steps and a scan speed of 1000 nm/min. Every sample was analyzed at least three times, the interval between measurements being 300 s.

The Beer-Lambert law shows the relation between the absorbance of the solution and the concentration of holmium ions:

$$Abs_\lambda = \varepsilon_\lambda \cdot l \cdot C \tag{3}$$

where Abs_λ is the absorbance value at a given λ wavelength [nm], ε_λ is the molar absorption coefficient [$dm^3\ cm^{-1}\ mol^{-1}$], l is the optically active path length [cm] and C is a concentration of Ho(III) ions [$moldm^{-3}$]. The values ε_λ and l are constant and known [15] so it is possible to define the relationship between the concentration and absorbance as linear.

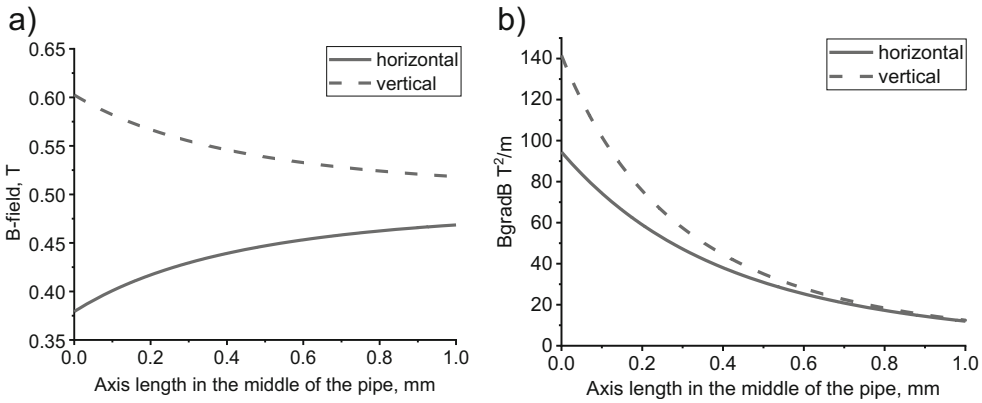

Fig. 6 Distribution of **a** the magnetic field $|\mathbf{B}|$, **b** the gradient of the magnetic field $|\mathbf{B}\nabla\mathbf{B}|$ along the axis of the pipe (dashed lines in Fig. 5)

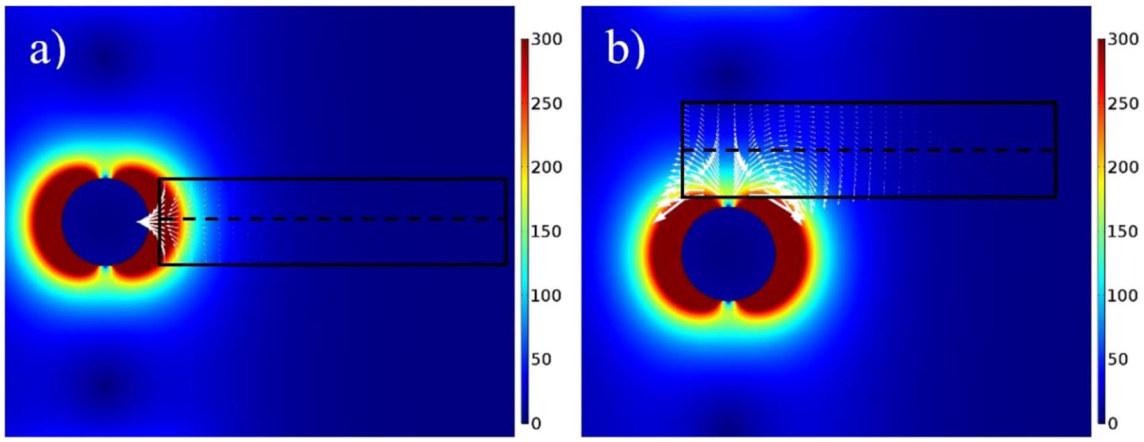

Fig. 7 Simulation of the magnetic field gradient $|\boldsymbol{B}\nabla\boldsymbol{B}|$ in T^2/m for: **a** Model 2 and **b** Model 3. The maximum value shown is limited to improve the presentation

The differences in the Ho(III) ions concentration from the two outputs were calculated as follows:

$$\Delta C_{i,j} = \frac{Abs_{output1,i,j} - Abs_{output2,i,j}}{Abs_{output1,i,j}} \times 100\% \quad (4)$$

where $Abs_{output1}$ and $Abs_{output2}$ are the mean values of absorbance from outputs 1 and 2, i – number of samples, j – number of repetitions of UV-Vis measurement. The output near the iron wire is marked as 1. The second – further away from the wire – is marked as output 2. The mean value of the change in the concentration was calculated as:

$$\overline{\Delta C} = \frac{\sum \Delta C_{i,j}}{i \times j} \quad (5)$$

The standard deviation was calculated as:

$$\sigma = \sqrt{\frac{1}{i \times j - 1} \sum \left(\Delta C_{i,j} - \overline{\Delta C}\right)^2} \quad (6)$$

In the case of the cascade (set of three Model 1 cells), outputs number 1 and 3 were analyzed as they were respectively expected to display the biggest difference in the concentration of holmium ions (Fig. 4).

Results

The mean difference in the concentration was calculated based on the absorbance at two peak wavelengths – 537 and 641 nm.

Figure 10 contains examples of graphs presenting the way the concentration differences between two outputs were calculated. The results shown here are from the experiment carried out in the Model 1 cell. The mean value of absorbance is presented for the samples collected from output 1 and output 2. Results are shown for all the samples collected at different flow rate values. The error bars show the standard deviation (± σ) in the absorbance of the sample for repetitions of the spectrum measurements.

The results presented in Fig. 10 show the differences in concentration between two outputs. In this case, a higher concentration is expected to be obtained in the solution from output 1 due to the gradient of the magnetic field. However, this relation is not observed in all samples. Generally, the error

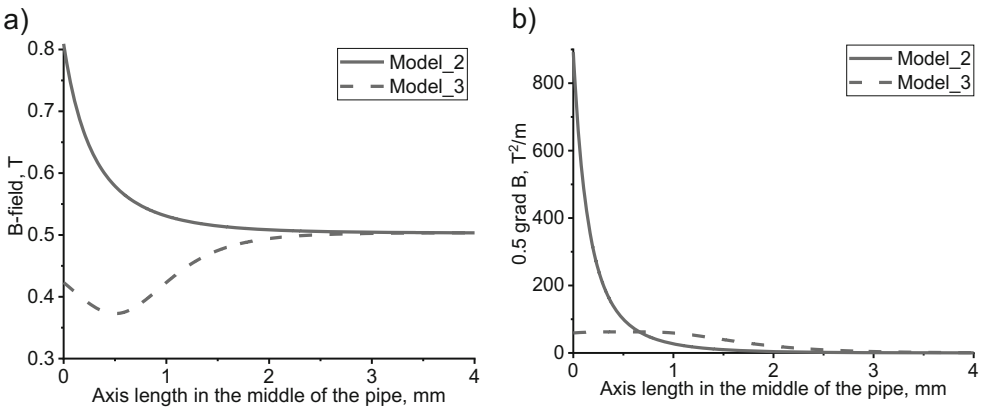

Fig. 8 Distribution of **a** the magnetic field $|\mathbf{B}|$, **b** the gradient of the magnetic field $|\mathbf{B}\nabla\mathbf{B}|$ along the axis of the pipe (dashed lines in Fig. 7)

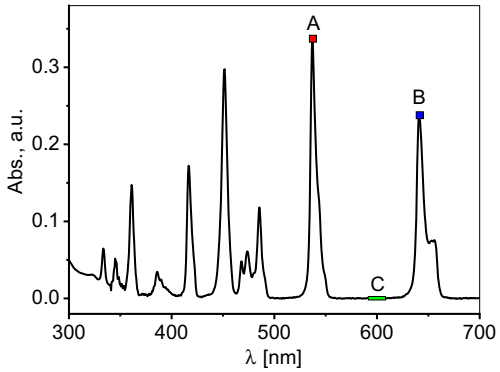

Fig. 9 An example UV-Vis spectrum for a 0.1 M holmium solution. The square markers A at 537 nm and B at 641 nm denote the relevant maxima of the analyzed spectrum. The rectangular marker C at 590–610 nm is used to correct the spectrum

bars are smaller than the concentration differences, though not in all cases. The changes in the absorbance between samples at different flow rates arise because the new portion of input solution is used.

Figure 11 shows the differences in concentration between two outputs compared to the flow rate. The absorption values were averaged for every flow rate. According to the simulations, positive value of ΔC are expected to be obtained in Model 1, Model 2 and the cascade. A decrease in the concentration is expected in Model 3. However, the error bars are bigger than the mean concentration differences.

In Model 1, the value of ΔC is varied from −0.4 to 0.4% for different flow rates. The difference in concentration increases with the flow rate; for 10 ml/h it is a negative value, for 100 ml/h it is positive. The mean changes in the concentration obtained in the experiments in the Model 1 cell are positive in most cases, while at lower flow rates there are negative values of concentration differences. Also, different tendencies are observed between curves based on two wavelengths – 537 and 641 nm at flow rates equal to 20 and 100 ml/h. In the first case the difference is greater at 641 nm, in contrast to the results obtained at a 100 ml/h flow rate.

In Model 2 and Model 3, the mean changes in the concentration are smaller than the error bars. On one hand, the values of the error bars at a faster flow are probably bigger due to local turbulent flows of the solution in the channel. On the other hand, at a low flow rate the errors come from differences in pressure from the two outputs. In both cases, the differences are negative independently of the flow rate. In Model 3, a negative value of difference was observed.

In the cascade of three Model 1 cells, the ΔC value is positive for a 10 ml/h flow rate and negative for 60 ml/h.

The mean value of the standard deviation is 0.28% and the highest value is 0.78%. These values are satisfying due to the high accuracy obtained when using the analytical method.

Table 1 presents the conditions and results of every experiment.

Discussion

In the following, further aspects which might have influenced our results are discussed:

Laminar flow and channel curvature

To achieve separation, the flow in the pipe and channel needs to be laminar. An important dimensionless parameter for characterizing the flow is the Reynolds number, which is defined as $Re = \frac{U \times L}{\nu}$ where U denotes the velocity of flow, L a characteristic length scale, e.g. the diameter of the pipe, and ν the kinematic viscosity of the solution. For laminar flow, a parabolic profile in the pipes can be assumed (Table 2).

The calculated Reynolds number values are satisfying, as they confirm that the flow of the solution inside the channel is laminar. Due to the bigger cross-sectional area of the rectangular channel, in this case the Reynolds number is smaller than in the channel with a circular cross section. It is seen that the Reynolds numbers are far below the critical Reynolds number of about 1000 where a transition to turbulence usually starts.

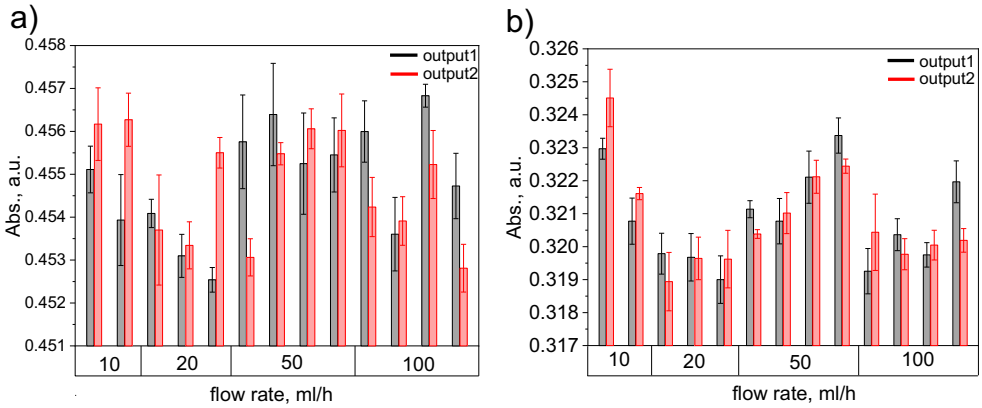

Fig. 10 The absorbance values at both outputs for different flow rates from Model 1 at: **a** 537 nm, **b** 641 nm wavelength. The external magnetic field is 0.920 T

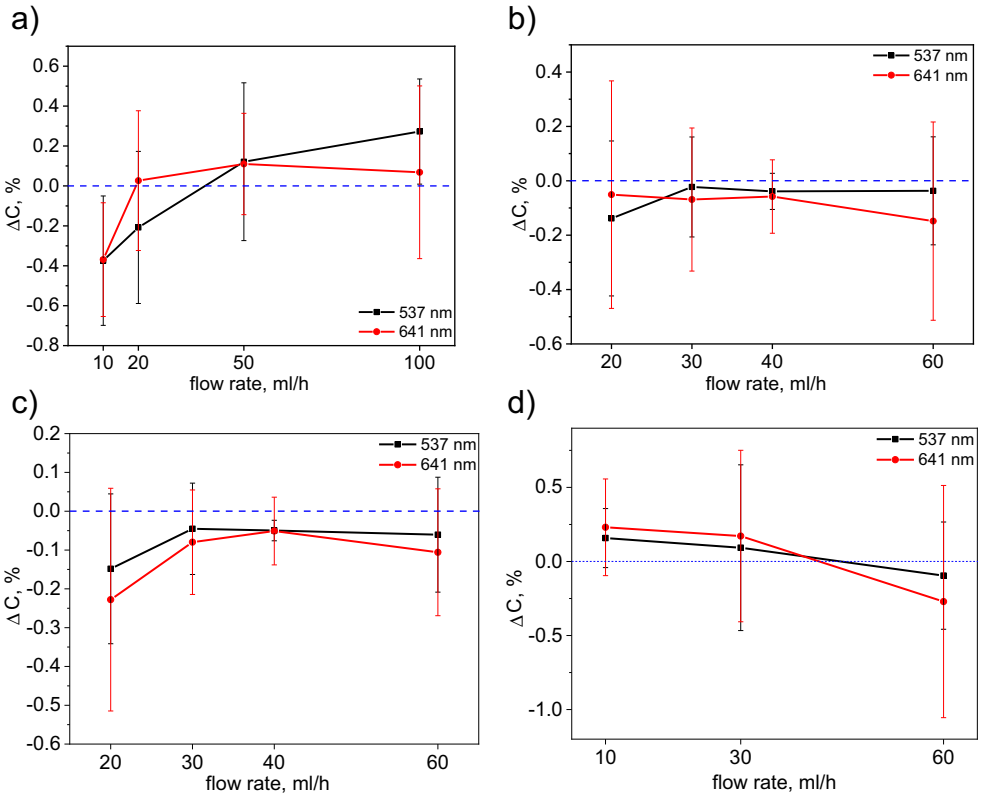

Fig. 11 Differences in the Ho(III) ion concentration in **a** Model 1 (applying a magnetic field of 0.920 T), **b** Model 2 (0.600 T), **c** Model 3 (0.600 T), **d** cascade (0.300 T)

To evaluate the influence of the curvature of the channel on transition, the Dean number should be considered, which can be defined as $De = Re\frac{s}{2r}^2$. Here, r denotes the radius of curvature and s denotes the pipe diameter. For Dean numbers smaller than 54, the curvature does not lead to vortices driven by a centrifugal force which would then remix the solution [25, 26]. As in our case, for the spiral channel r>>s and Re<35; the stability criterion is fulfilled in all cases.

Table 1 Results of the experiments

Model of cell	Magnetic field, T	Flow rate, ml/h	Number of		Results for 537 nm		Results for 641 nm	
			Samples (i)	Measurement repetition (j)	$(\overline{\Delta C})$, %	(σ), –	$(\overline{\Delta C})$, %	(σ), –
Model 1	0.920	10	2	5	−0.37421	0.32417	−0.36905	0.28492
		20	3	5	−0.20785	0.38104	0.02662	0.35012
		50	4	5	0.12139	0.39537	0.11005	0.25381
		100	4	5	0.27253	0.26348	0.06837	0.43261
Model 2	0.600	20	5	3	−0.1385	0.28492	−0.0509	0.41829
		30	9	3	−0.02269	0.18391	−0.06894	0.26313
		40	4	1	−0.03892	0.06637	−0.05783	0.13508
		60	3	3	−0.03698	0.19861	−0.14828	0.36462
Model 3	0.600	20	4	3	−0.14834	0.19306	−0.22787	0.28696
		30	7	3	−0.04537	0.11771	−0.0798	0.13458
		40	4	1	−0.04967	0.0264	−0.05106	0.08731
		60	4	3	−0.06044	0.14812	−0.10578	0.16347
cascade	0.300	10	3	2	0.15799	0.19949	0.23078	0.32654
		30	4	2	0.09287	0.55988	0.17161	0.57912
		60	8	2	−0.0957	0.36195	−0.27084	0.78392

Table 2 Velocity and Reynolds number at different flow rates

Flow rate [ml/h]	Circular channel		Rectangular channel	
	Velocity [mm/s]	Re	Velocity [mm/s]	Re
10	3.54	3.54	0.694	0.7
20	7.08	7.08	1.39	1.4
50	17.7	17.7	3.47	3.5
100	35.4	35.4	6.94	7.0

Wall roughness

Wall roughness may cause turbulence to occur earlier. A microscopic view of the channel surface is shown in the supplementary materials (Fig. S1), where confocal scanning microscopy was also used to analyze the surface of the printed cells (Fig. S2).

Figure 12a presents the SEM picture of the analyzed surface with three lines, while Fig. 12b shows profiles of the surface on three marked lines. The roughness parameter Ra obtained is equal to 4.6 ± 0.7 μm. For the random disturbances arising from this, due to the low Reynolds numbers mentioned above, viscosity is expected to clearly dominate in this near-wall layer and to avoid any additional cross-stream mixing of the flow. However, the flow in the rough wall layer, where the greatest enrichment is expected to occur, experiences elevated friction, which might additionally reduce the volume fraction of strongly enriched electrolyte at the outflow.

Besides, there are visible layers of hardened resin, the thickness of which is 50 μm. When carefully inspecting Fig. 12 and Fig. 2S of the supplementary material, nearly regular patterns of about this height are to be seen which arose from the 3D printing process. These pattern are oriented in a diagonal direction. Due to the spiral shape of the pipe/channel, the direction of these surface elevations with respect to the flow direction can be expected to periodically vary along the pipe/channel. As stated firstly in [28, 29], such patterns may trigger a crossflow, which then could lead to mixing processes faster than molecular diffusion. However, the relative height of the surface pattern with respect to pipe/channel height amounts to 5% only in our case, whereas available data in literature typically refer to about 20–30%. Therefore, a direct quantitative estimation of the effect appears difficult and has to be left to future investigations.

Influence of gravity

As shown in Figs. 3 and 4, the magnetic enrichment is intended to take place horizontally. However, the enrichment of species leads to an increase in the density of the electrolyte. Gravity could force a convection in the cross section of the channel which would counter-influence the intended enrichment in the left and right parts of the channel. In order to check the relevance of this, we estimate both forces. As the density changes are small, in the range of a Boussinesq approximation for the gravity only the changes in density can contribute to convection. The force density is:

$$\boldsymbol{f_G} = \Delta\rho \cdot \boldsymbol{g} \tag{7}$$

where $\boldsymbol{g}$ denotes the constant of gravitational acceleration. For the magnetic gradient force, only the change in the susceptibility of the electrolyte needs to be taken into account [27].

$$\boldsymbol{f_B} = \frac{\Delta\chi_{sol}}{\mu_0}\boldsymbol{B}\nabla\boldsymbol{B} \tag{8}$$

Here, μ_0 denotes the magnetic field constant of a vacuum. Assuming a maximum relative enrichment of 10% from a 0.1 M solution for both forces, the change in the density amounts to about 1.5 kg/m^3, and the change in the susceptibility of the holmium solution amounts to about.

10^{-5}. When the magnetic field times its gradient is assumed to be about 10^3 T^2/m, the gradient force can be estimated as 10^4 N/m^3, whereas the gravity force amounts to only about 15

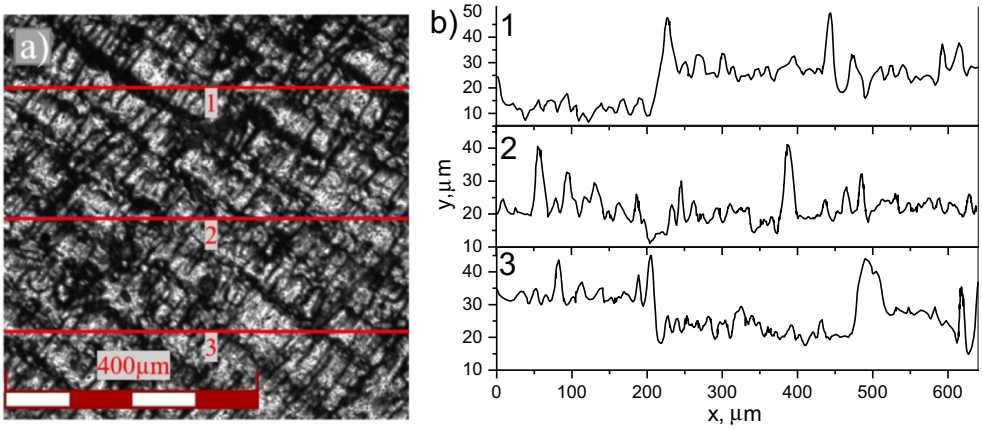

Fig. 12 Analysis of roughness: **a** SEM picture of the surface **b** roughness profiles along three lines marked in red color

N/m^3. As the magnetic gradient force clearly dominates, the influence of gravity can be safely ignored.

Mixing by diffusion

The magnetic enrichment caused by the magnetic gradient force is counter-influenced by diffusion. Therefore, the time of magnetic exposure should not be too long. A characteristic time-scale of cross-flow diffusion can be estimated as

$$\tau = \frac{L^2}{D} \tag{9}$$

where L and D denote a characteristic length scale (channel width) and the diffusion coefficient, respectively. For 1 mm and 10^{-9} m^2/s, the time amounts to about 10^3 s, which is longer than the time the solution needs to flow through the channel even at the smallest flow rate.

Conclusions

The present work involved an attempt to dynamically separate rare-earth metal ions in an aqueous solution using inhomogeneous magnetic fields. The aim was to obtain a continuous flow method based on the different magnetic susceptibilities of the ions. Holmium was used as it has the highest magnetic moment of all rare-earth metal ions.

The first step was to analyze the transport of the individual metal ions. The separation processes are based on the gradient of the magnetic field, which generates the magnetic force responsible for the transportation of ions. The gradient of the magnetic field is obtained using an iron wire in a homogeneous magnetic field. The position and geometry of microflow cells are optimized by numerical simulation of the magnetic field and the gradient of the magnetic field in the cross section of the channel.

This work used an aqueous solution of 0.1 M Ho(III). The solution pH was adjusted to 1 to avoid the secondary precipitation of holmium compounds. Microcells were used which were made from light hardened resins applying the technology of 3D printing. A channel with a small cross section ensures that a laminar flow is obtained inside. Also, it is recommended to apply a low speed of flow to maximize the time for the magnetic field attraction of ions.

Three types of microflow cells were tested – one with a circular channel and two with rectangular channels. Additionally, a set of three cells with circular channels were used. All of them were placed perpendicularly in the homogeneous magnetic field generated by the electromagnet. The holmium solution was pumped through the cell and, at the end of the channel, it was divided into four streams and 4 ml samples were collected. The samples were repeatedly measured using UV-Vis spectroscopy and the differences in concentration between them were calculated.

While differences in absorbance from the outputs are observed, these values generally include error margins. Unfortunately, despite the relatively high accuracy of the analysis method applied, the error margins are of the same range or even larger than the enrichment effect observed. Thus, a clear statement about the separation efficiency can not be drawn and has to be left for future work and possibly improved devices. As discussed above, adsorption, surface roughness or the curvature of the flow in the spiral are not expected to be detrimental. However, as also mentioned in the discussion section, due to the 3D printing process used for manufacturing the spiral flow cell, quasi regular surface elevations of changing direction appear at the walls, which might trigger crossflow mixing that would reduce the magnetic separation effect. With respect to further optimization of the cell, we intend to continue this investigation in the near future with microflow cells of smoothened inner walls, improved geometry and by applying a higher gradient of the magnetic field to obtain also stronger magnetic gradient force.

Acknowledgements The authors wish to acknowledge the German Federal Ministry of Education and Research BMBF under project number 01DS16007 for financial support. The Polish team wishes to acknowledge the Polish National Science Center [grant number 2014/15/B/ST8/01528] for financial support. We are thankful to professor Beata Leszczynska-Madej for her analysis of the roughness of printed cells, professor Kerstin Eckert for discussions and Drs. Dirk Räbiger and Klaus Timmel for their support with the electromagnet.

Compliance with ethical standards

Conflict of interest On behalf of all authors, the corresponding author states that there is no conflict of interest.

References

1. Saias L, Saliba A-E, Pierga J-Y , Vielh P, Farace F, Viovy J-L (2008), Microfluidic magnetic cell sorting system for cancer diagnosis, Twelfth International Conference on Miniaturized Systems for Chemistry and Life Sciences October 12–16, 2008, San Diego, California, USA, 552–554
2. Hirschbein BL, Brown DW, Whitesides GM (1982) Magnetic separation in chemistry and biochemistry. Chemtech 12:172–179
3. Safarik I, Safarikova M (2009) Magnetic nano- and microparticles in biotechnology. Chem Pap 63:497–505
4. Berensmeier S (2006) Magnetic particles for the separation and purification of nucleic acids. Appl Microbiol Biotechnol 73:495–504

5. Inglis DW, Riehn R, Sturm JC, Austin RH (2006) Microfluidic high gradient magnetic cell separation. J Appl Phys 99:08K101
6. Ambashta RD, Sillanpää M (2010) Water purification using magnetic assistance : a review. J Hazard Mater 180:38–49
7. Borghi CC, Fabbri M, Fiorini M, Mancini M, Ribani PL (2011) Magnetic removal of surfactants from wastewater using micrometric iron oxide powders. Sep Purif Technol 83:180–188
8. Mariani G, Fabbri M, Negrini F, Ribani PL (2010) High-gradient magnetic separation of pollutant from wastewaters using permanent magnets. Sep Purif Technol 72:147–155
9. Sinha A, Ganguly R, Puri IK (2009) Magnetic separation from superparamagnetic particle suspensions. J Magn Magn Mater 321: 2251–2256
10. Arppe RO, Salovaara L, Mattsson S, Lahtinen T, Valta TR, Soukka T (2013) High gradient magnetic separation of upconverting lanthanide nanophosphors based on their intrinsic paramagnetism. J Nanopart Res 15:1883
11. Ji B, Wu P, Ren H, Zhang S, Rehman A, Wang L (2016) Segregation behavior of magnetic ions in continuous flowing solution under gradient magnetic field. Chinese Phys B 25:074704
12. Pulko B, Yang X, Lei Z, Odenbach S, Eckert K (2014) Magnetic separation of Dy(III) ions from homogeneous aqueous solutions. Appl Phys Lett 105:232407
13. Yang X, Tschulik K, Uhlemann M, Odenbach S, Eckert K (2014) Magnetic separation of paramagnetic ions from initially homogeneous solutions. IEEE Trans Magn 50:4600804
14. Kolczyk K, Kutyla D, Wojnicki M, Cristofolini A, Kowalik R, Zabinski P (2016) Separation of rare earth metals ions in a static magnetic field. Magnetohydrodynamics 52:541–547
15. Kołczyk K, Wojnicki M, Kutyła D, Kowalik R, Zabiński P, Cristofolini A (2016) Separation of Ho^{3+} in static magnetic field. Arch Metall Mater 61:1919–1924
16. Franczak A, Binnemans K, Fransaer J (2016) Magnetomigration of rare-earth ions in inhomogeneous magnetic fields. Phys Chem Chem Phys 18:27342–27350
17. Rodrigues I, Lukina L, Dehaeck S, Colinet P, Binnemans K, Fransaer J (2017) Magnetomigration of rare-earth ions triggered by concentration gradients. J Phys Chem Lett 21:5301–5305
18. Binnemans K, Jones PT, Blanpain B, Van Gerven T, Yang Y, Walton A, Buchert M (2013) Recycling of rare earths: a critical review. J Clean Prod 51:1–22
19. Grandell L, Lehtil A, Kivinen M, Koljonen T, Kihlman S, Lauri LS (2016) Role of critical metals in the future markets of clean energy technologies. Renew Energy 95:53–62
20. Massari S, Ruberti M (2013) Rare earth elements as critical raw materials: focus on international markets and future strategies. Res Policy 38:36–43
21. Yoon HS, Kim CJ, Chung KW, Kim SD, Lee JY, Kumar JR (2016) Solvent extraction, separation and recovery of dysprosium (Dy) and neodymium (Nd) from aqueous solutions: waste recycling strategies for permanent magnet processing. Hydrometallurgy 165:27–43
22. Wang J, Chen G, Xu S, Yin Z, Zhang Q (2016) Solvent extraction of rare earth ions from nitrate media with new extractant di-(2,3-dimethylbutyl)-phosphinic acid. J Rare Earths 34:724–730
23. Lei Z, Fritzsche B, Eckert K (2017) Evaporation-assisted magnetic separation of rare-earth ions in aqueous solutions. J Phys Chem C 121:24576–24587
24. Noddack I, Wicht E (1955) Trennung der seltenen Erden im inhomogenen Magnetfeld. Chem Tech 7:3–5
25. Dean WR (1928) Fluid motion in a Curved Channel. Proc R Soc 84:402–420
26. Hammerlin G (1957) Die Stabilitaet der Stroemung in einem gekriimmten Kanal. Arch Ration Mech Anal 1:212–224
27. Strook A, Dertinger S, Ajdari A, Mezic I, Stone H, Whitesides G (2002) Chaotic mixer for microchannels. Science 295:647–651
28. Lynn N, Dandy D (2007) Geometrical optimization of helical flow in grooved micromixers. Lab Chip 7:580–587
29. Mutschke G, Tschulik K, Weier T, Uhlemann M, Bund A, Fröhlich J (2010) On the action of magnetic gradient forces in microstructured copper deposition. Electrochim Acta 55:9060–9066